ARTICLES

# Novel Photoluminescence Properties of Magnetic Fe/ZnO Composites: Self-Assembled ZnO Nanospikes on Fe Nanoparticles Fabricated by Hydrothermal Method

**Z. X. Yang,[†] W. Zhong,*[,†] C. T. Au,[‡] X. Du,[†] H. A. Song,[†] X. S. Qi,[†] X. J. Ye,[†] M. H. Xu,[†] and Y. W. Du[†]**

*Nanjing National Laboratory of Microstructures and Department of Physics, Nanjing University, Nanjing 210093, People's Republic of China, and Chemistry Department, Hong Kong Baptist University, Hong Kong, People's Republic of China*

*Received: April 5, 2009; Revised Manuscript Received: October 29, 2009*

Magnetic Fe/ZnO composites showing the shape of "sea urchin" have been hydrothermally synthesized at 80 °C. The Fe nanoparticles are encapsulated inside a shell of self-assembled ZnO nanospikes. The Fe/ZnO composites display photoluminescence properties different from those of the ZnO entities generated similarly but in the absence of Fe powder: (i) a UV emission band is observed over the latter but not over the former, and (ii) the former shows an emission peak around 583 nm (wavelength) with intensity significantly stronger than that of the latter. Because of the encapsulation of the Fe nanoparticles, the Fe/ZnO composites are stable in air and high in magnetization.

## Introduction

Zinc oxide (ZnO) is a cheap semiconductor and is known to be environmentally friendly. The nanostructures (such as nanowires,[1] nanosbelts,[2] nanotubles,[3] nanorings,[4] nanobows,[5] nanohelixes[6]) of ZnO have been synthesized and studied in the past decade. The materials have a wide band gap (3.37 eV), large exciton binding energy (60 meV), large electron mass 0.3 $m_e$ ($m_e$: bare electron mass), and excellent chemical and thermal stability, and have been widely studied in terms of its catalytic,[7] optoelectronic,[8] and photoelectrochemical[9] properties. In photocatalytic decolorization,[7] with the introduction of a magnetic material to ZnO, the separation of a ZnO-based catalyst from the reaction medium would be easy in a magnetic field.

In the domain of bioengineering, ZnO has been investigated for growth prohibition of *Saccharomyces cerevisiae*,[10] bacteria,[11] and microalgae.[12] Also, being biodegradable and biocompatible, ZnO wires are used in biosensors and biological systems.[13] With the awareness of the anticancer effect of photoexcited ZnO,[14] the guided delivery of ZnO-based drugs has become a topic of interest. It is envisaged that magnetic ZnO composites in the form of capsules or nanosubmarines can be magnetically guided to a desired location of a human body. As a result, there would be significant enhancement of ZnO efficiency and large reduction in dosage and cost.

To synthesize Fe/ZnO core−shell composites at low temperatures through a simple method has been a challenge to researchers. Herein, we report the hydrothermal synthesis of magnetic Fe/ZnO composites with ZnO nanospikes self-assembled on the surface without the use of a surfactant. The approach is efficient, and the outcome is highly reproducible. The synthesis is conducted at low temperature (80 °C), and there is no need of using a surfactant. To the best of our knowledge, the fabrication of such kind of Fe/ZnO composites has never been reported before.

## Experimental Section

All of the reagents used in this study were of analytical grade (purchased from Shanghai Chemical Industrial Co.) and used without further purification. For the synthesis of the Fe/ZnO composites, 14.87 g of zinc nitrate [$Zn(NO_3)_2 \cdot 6H_2O$] and 40.0 g of NaOH were dissolved in deionized water to form a 100.0 mL solution. Next, 3.0 mL of the solution was mixed with 5.0 mL of deionized water and 25.0 mL of absolute ethanol ($C_2H_5OH$), followed by the addition 5.0 mL of ammonia (25%). Before being transferred into a Teflon-lined autoclave, 0.84 g of Fe powder (armco iron, 3zhp) was added, and the resulted mixture was stirred vigorously for several minutes. The autoclave with its content was then left in an electric oven at 80 °C for 3, 10, or 24 h. For comparison, ZnO was produced using the above 24 h procedure but without the introduction of Fe powder. At the end of hydrothermal treatment, the as-prepared solid material was separated using a centrifuge and was thoroughly washed in three cycles of absolute ethanol and deionized water.

The samples were examined on an X-ray powder diffractometer (XRD) at room temperature for phase identification using Cu Kα radiation (model D/Max-RA, Rigaku, Japan). The surface components of the products were studied by a VG ESCALAB MKII X-ray photoelectron spectrometer (XPS) at 1.0 eV resolution using Al Kα radiation ($h\nu = 1486.6$ eV). The bulk contents of the composites were determined by induced coupled plasma (ICP) spectroscopy (model 1100 + 2000, Jarrell-Ash, USA). The morphology of the samples was examined over

* Corresponding author. Tel.: +86-25-83621200. Fax: +86-25-83595535. E-mail: wzhong@mail.nju.edu.cn.
[†] Nanjing University.
[‡] Hong Kong Baptist University.

10.1021/jp903130t 
Published on Web 11/25/2009

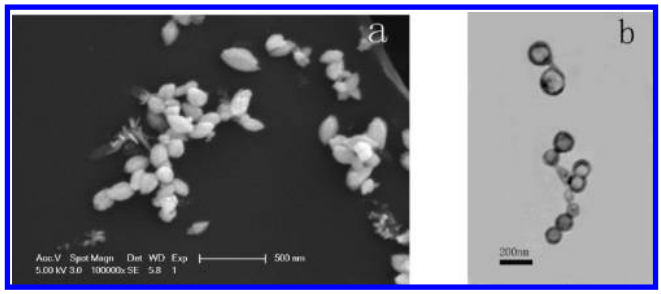


**Figure 1.** (a) FE-SEM and (b) TEM images of as-synthesized ZnO.

a transmission electron microscope (TEM) operated at an accelerating voltage of 80 kV and a field-emission scanning electron microscope (FE-SEM model FEI Sirion 200, America) operated at an accelerating voltage of 5 kV. Magnetic measurements were performed at room temperature using a vibrating sample magnetometer (VSM) (Lakeshore, USA). The photoluminescence (PL) was measured at room temperature using a He−Cd laser (excitation source: 325 nm).

## Results and Discussion

Figure 1 shows the FE-SEM and TEM images of the ZnO crystallites generated without the introduction of Fe powder. According to the FE-SEM image (Figure 1a), the ZnO particles are in the form of ellipsoids and display a statistical diameter and length of ca. 150 and 250 nm, respectively. From the TEM image (Figure 1b), one can see that the ellipsoids are hollow with size of 150−200 nm, in line with the result of Figure 1a. In other words, without the introduction of Fe powder, the product of hydrothermal synthesis is hollow ZnO ellipsoids. It was reported that during the growth of ZnO entities, preferential chemical dissolution of the metastable (0001) faces would take place, leading to hollow structures in the aging process.[15] In other words, with extension of aging time, there would be an increase in dissolution rate at the interface of twinning subunits. In our system, this is accompanied by the energetically favorable self-assembly of newly formed nanoparticles as well as the Ostwald ripening process that involves the transformation of the smaller nanoclusters from inside toward the outside.[16] As a result, hollow ZnO ellipsoids are formed.

Displayed in Figure 2 are the FE-SEM images of raw Fe particles and Fe/ZnO composites collected after 3, 10, and 24 h of hydrothermal treatment. The FE-SEM image of Fe powder (armco iron, 3zhp) used as raw material is shown in Figure 2a. It is worth noting that the Fe particles are irregular in shape, and with sizes ranging from 10 to 50 $\mu$m. One can see that the Fe/ZnO composites collected after 3 h of hydrothermal treatment show the shape of "sea urchin", having size in the 2−2.5 $\mu$m range (Figure 2b). After 10 h, the size of Fe/ZnO composites reduces to 0.7−1 $\mu$m (Figure 2c), and after 24 h, the size further declines to about 300 nm (Figure 2d). It is obvious that with time of hydrothermal treatment, there is gradual diminution of size plausibly due to the causticization of metallic iron in the alkali solution. Nevertheless, despite the difference in size, the samples obtained at different synthesis times are uniform in morphology.

Depicted in Figure 3 are the TEM images of the 3, 10, and 24 h Fe/ZnO composites. It is clear that the 3 and 10 h Fe/ZnO composites show the shape of "sea urchin", and the surface is covered with nanospikes. The "sea urchins" collected after 3 h exhibit good monodispersion, having size in the 2−2.5 $\mu$m range. After 10 h, the size of Fe/ZnO composites is in the 700−1000 nm range (Figure 3b). The Fe/ZnO composites collected after 24 h show preferential growth along certain directions (Figure 3c).

Figure 4 shows the results of phase identification by XRD. The patterns show lines corresponding to α-Fe and wurtzite ZnO. Because there is no detection of other phases, we deduce that the as-fabricated samples are composed of α-Fe and ZnO. With prolonged treatment (from 3 to 24 h), the ZnO peaks enhance in intensity, and the (100), (002), and (101) peaks become clearly visible (Figure 4b). On the basis of the results of FE-SEM, TEM, and XRD analyses, one can deduce that the "sea urchin" samples are composed of α-Fe and wurtzite ZnO.

The surface composition of the Fe/ZnO composite collected after 24 h of hydrothermal treatment was investigated by means of XPS analysis, and the results are shown in Figure 5. Figure 5a is the survey scan, and the peaks can be ascribed to Zn, O, Fe, and C elements. Figure 5b shows the Fe2p signal. In addition to the peaks of $Fe2p_{1/2}$ (at 710.2 eV) and $Fe2p_{3/2}$ (at 724.1 eV), a satellite peak at 717.7 eV is observed; similar features were reported in the case of $\gamma$-$Fe_2O_3$.[17] The data give strong indication of the presence of $Fe^{3+}$. As revealed by quantitative analysis, the surface Zn:O:Fe composition is 31.95:35.08:1.96, giving a surface Fe/Zn ratio of 0.06/1, much lower than that of the bulk (Fe/Zn ratio = 7.12/1) estimated in ICP measurement. The results so far suggest that the Fe/ZnO composites are core/shell structured, with the Fe cores covered by ZnO nanospikes. It is worth pointing out that the $Fe2p_{1/2}$ peak around 710 eV should be ascribed to $Fe^{3+}$ ions rather than to metallic Fe. It is apparent that there is a minute presence of $Fe^{3+}$ ions on the surface of the Fe/ZnO composites. The $Fe^{3+}$ ions could exist as $Fe_2O_3$, $Fe(OH)_3$, or $Fe^{3+}$ ions incorporated in the lattice of the ZnO nanospikes. In ambient environment in the presence of water and oxygen, the oxidation (rusting) of Fe occurs. Under the condition of hydrothermal treatment in an autoclave at high pressure and high temperature, the rusting process would be facile. As a result of causticization, the metallic iron is etched and converted to $Fe_2O_3$ and $Fe(OH)_3$, as indicated by the reduction of particle size and a change of particle shape from irregular to spherical. Greene et al. reported the synthesis of ZnO-nanowire arrays using ZnO seeds.[18] We propose that upon the etching of the Fe particles, seeds of ZnO are accumulated on the surfaces of the Fe particles, and subsequently there is the growth of ZnO nanospikes. Because of the presence of $Fe^{3+}$ ions in the solution, it is possible to have $Fe^{3+}$ ions incorporated in the ZnO nanospikes during the growing process.

The magnetic hysteresis loops shown in Figure 6 are typical of soft magnetic materials. The coercivity of the samples is rather low, stretching from 8.4 to 9.5 Oe. The saturation magnetization ($M_S$) values of the composites collected after 3 and 24 h of hydrothermal treatment are 204 and 172 emu/g, respectively, not too far away from the $M_S$ (220 emu/g) of pure iron. The high $M_S$ confirms that it is metallic Fe rather than ferric oxide that exists inside the Fe/ZnO composites, in line with the results of XRD investigation. Over samples of the Fe/ZnO composites that had been exposed to air for over 3 months, we detected no changes in XRD features and magnetic properties (not shown). Overall, we find that the Fe/ZnO composites are stable in air and show relatively high magnetization. We believe that the high stability of the α-Fe nanoparticles in ambient environment is a result of entrapment of the α-Fe nanoparticles inside the ZnO nanospikes. To the best of our knowledge, such a kind of magnetic "sea urchin" (composed of self-assembled ZnO nanospikes and Fe nanoparticles) has never been reported before.

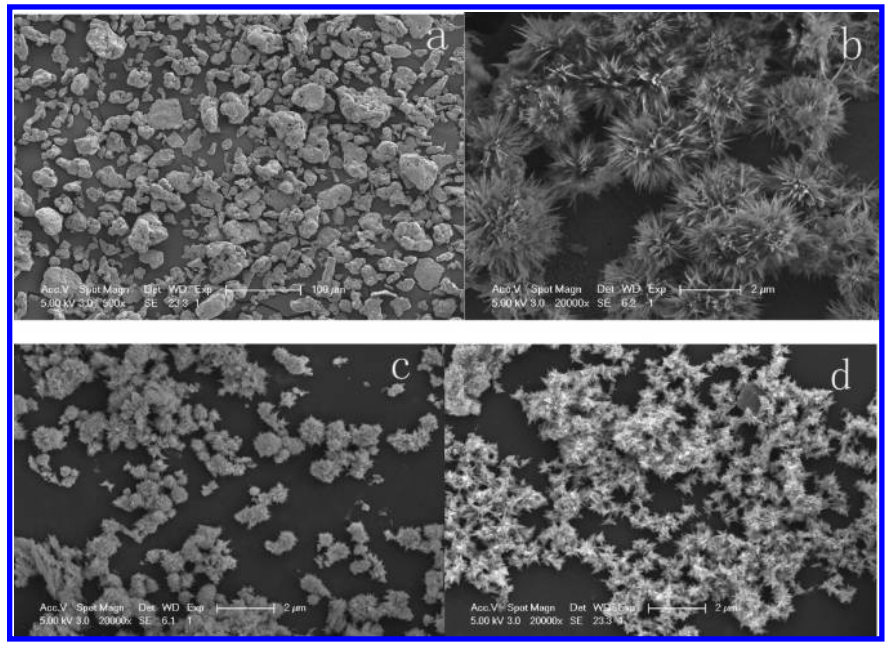


**Figure 2.** FE-SEM images of (a) Fe particles (raw material) and Fe/ZnO composites collected after (b) 3 h, (c) 10 h, and (d) 24 h of hydrothermal treatment at 80 °C.

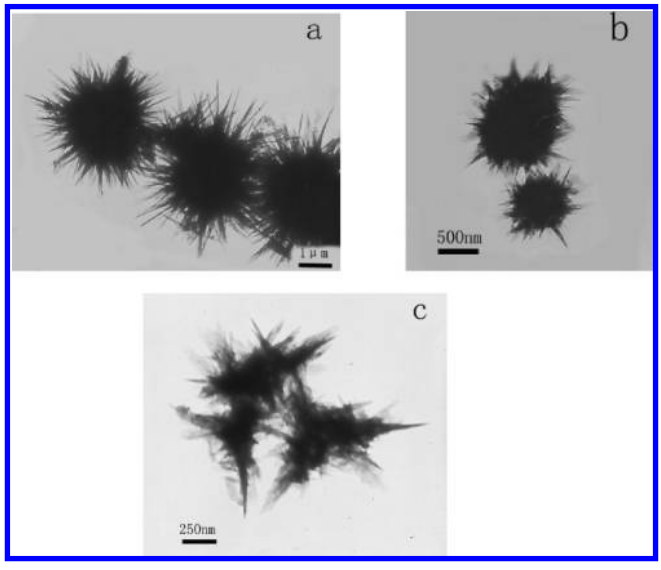


**Figure 3.** TEM images of Fe/ZnO composites collected after (a) 3 h, (b) 10 h, and (c) 24 h of hydrothermal treatment at 80 °C.

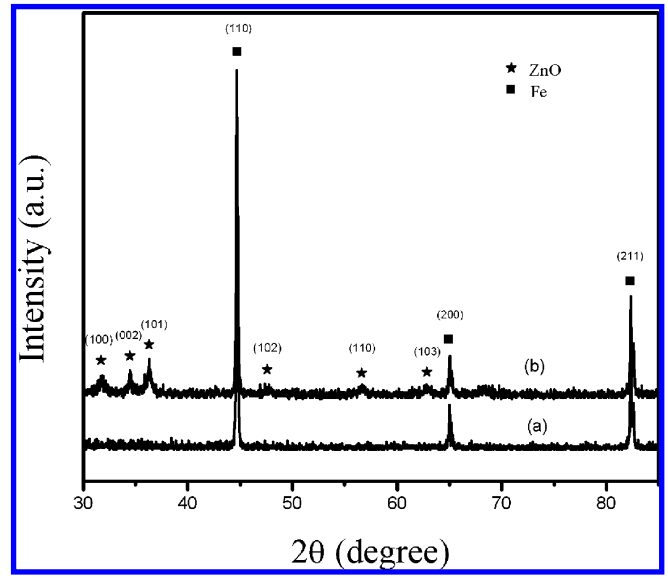


**Figure 4.** XRD patterns of Fe/ZnO composites collected after (a) 3 h and (b) 24 h of hydrothermal treatment at 80 °C.

The photoluminescence (PL) properties of the Fe/ZnO composites were studied at room temperature (Figure 7). An emission centered at 573 nm (green-yellow) and a narrow UV emission band at 385 nm attributable to the recombination of a hole in the valence band and an electron in the conduction band (excitonic emission) are detected over the ZnO ellipsoids (Figure 7a). It is considered that the green-yellow emission is originated from structural defects.[19] A comparison between spectra (b) and (a) of Figure 7 reveals that with the introduction of Fe particles, the UV emission band of ZnO undergoes red shift (from 385 to 408 nm), likely to be due to a size increase of the ZnO nanospikes (as shown in Figure 1b and Figure 3b). In addition, as compared to the PL of undoped ZnO, the green-yellow emission band of the Fe/ZnO composites also shows red shift (from 573 to 583 nm). The introduction of Fe nanoparticles into the ZnO matrix leads to a shift of both the PL defect band and the fundamental gap transition to lower energies. After 10 h of thermal treatment, there is no further red shift (yellow band), indicating that the defect density is relatively low and emission tuning is relatively small. With prolonged hydrothermal treatment, there is increase in the concentration of structural defects in ZnO, and hence remarkable enhancement of the relative intensity of the 583 nm band (Figure 7c). In Figure 7c, one can detect the disappearance of the UV emission band (at 385 nm) of ZnO and large intensity rise of the 583 nm band. As suggested by Bhatti et al.,[20] the quenching of the UV emission band could be due to the Fe ions in ZnO that act as a quencher. The yellow emission of Fe-doped ZnO can be assigned to the transition between energy levels of $Fe^{3+}$ ions; a similar phenomenon has been observed by Guo et al. over Mn-doped ZnO nanocrystals.[21] The intensity increase of yellow emission with time of hydrothermal treatment is a result of enhanced pervasiveness of $Fe^{3+}$ in ZnO. With sharp rise of mismatch between $Zn^{2+}$ and $Fe^{3+}$, there is a significant increase in structural defects in the Zn lattice. As pointed out by Oh et al., this could be a key reason for the large yellow emission observed over core−shell Fe/ZnO

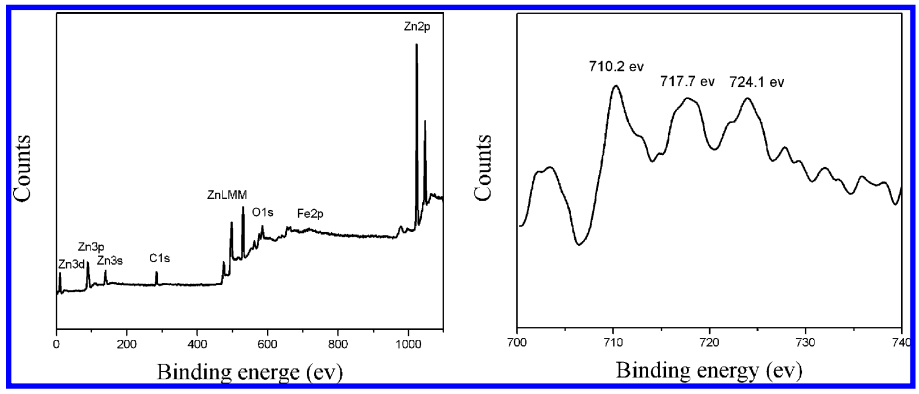


**Figure 5.** XPS spectra of Fe/ZnO composites collected after 24 h of hydrothermal treatment at 80 °C: (a) full scan and (b) Fe2p spectrum.

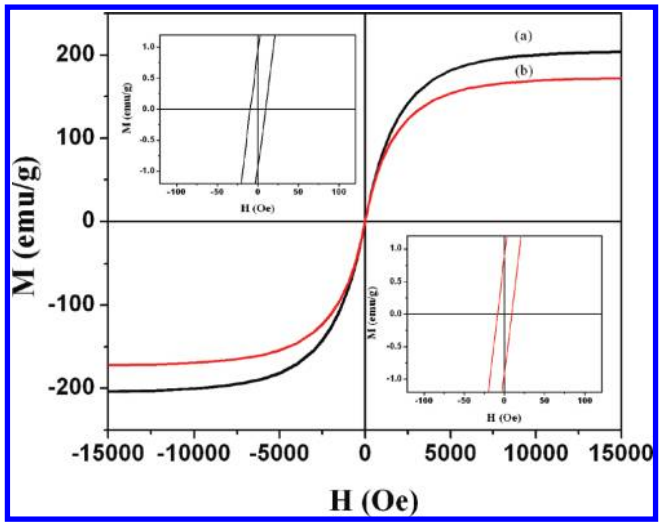


**Figure 6.** Room-temperature magnetic hysteresis loop of Fe/ZnO core/shell composites collected after (a) 3 h and (b) 24 h of hydrothermal treatment.

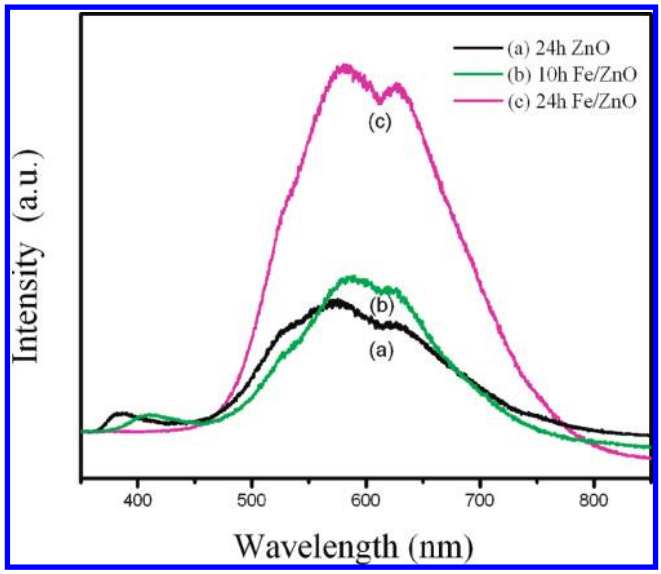


**Figure 7.** PL spectra of (a) ZnO hollow ellipsoids and (b,c) Fe/ZnO composites collected after 10 and 24 h of hydrothermal treatment, respectively.

crystals.[22] It is deduced that the ZnO of the Fe/ZnO composites is doped with $Fe^{3+}$ ions, and the concentration of structural defects in the Fe/ZnO composites is higher than that in the ZnO hollow ellipsoids.

## Conclusions

We have demonstrated that by means of a facile and low-cost hydrothermal approach, magnetic core−shell Fe/ZnO composites can be fabricated at 80 °C without the use of a surfactant. On the basis of the results of FESEM, TEM, XRD, and XPS investigations, we come to the deduction that the Fe nanoparticles are coated by ZnO nanospikes. With the incorporation of $Fe^{3+}$ ions inside the ZnO lattice, the UV emission band of ZnO disappears, and the defect-related peak centered at ca. 583 nm becomes strong in intensity. The results reveal that the PL properties of ZnO can be tuned by doping ZnO with $Fe^{3+}$ ions. The Fe/ZnO composites with the shape of sea urchin are stable in air and show relatively high magnetization due to the entrapment of α-Fe nanoparticles inside the ZnO nanospikes.

**Acknowledgment.** This work was supported by the National Natural Science Foundation of China (Grant No. 10674059), the National High Technology Research and Development Program of China (Grant No. 2007AA021805), and the National Key Project for Basic Research (Grant No. 2005CB623605), People's Republic of China.

## References and Notes

(1) Huang, M. H.; Wu, Y. Y.; Feick, H.; Tran, N.; Weber, E.; Yang, P. D. *Adv. Mater.* **2001**, *13*, 113.
(2) Pan, Z. W.; Dai, Z. R.; Wang, Z. L. *Science* **2001**, *291*, 1947.
(3) Gui, Z.; Liu, J.; Wang, Z. Z.; Song, L.; Hu, Y.; Fan, W. C.; Chen, D. Y. *J. Phys. Chem. B* **2005**, *109*, 1113.
(4) Kong, X. Y.; Ding, Y.; Yang, R.; Wang, Z. L. *Science* **2004**, *303*, 1348.
(5) Hughes, W. L.; Wang, Z. L. *J. Am. Chem. Soc.* **2004**, *126*, 6703.
(6) Gao, P. X.; Ding, Y.; Mai, W. J.; Hughes, W. L.; Lao, C. S.; Wang, Z. L. *Science* **2005**, *309*, 1700.
(7) Sivakumar, T.; Shanthi, K.; Newton Samuel, T. *Bioprocess Eng.* **2000**, *23*, 579.
(8) Lee, S. W.; Jeong, M. C.; Myoung, J. M. *Appl. Phys. Lett.* **2007**, *90*, 133115.
(9) Lopez, C. M.; Choi, K. S. *Abstr. Pap. Am. Chem. Soc.* **2004**, *227*, U1310.
(10) Kasemets, K.; Romet, M.; Ivask, A.; Kahru, A. *Toxicol. Lett.* **2008**, *180S*, S223.
(11) Heinlaan, M.; Ivask, A.; Blinova, I.; Dubourguier, H. C.; Kahru, A. *Chemosphere* **2008**, *71*, 1308.
(12) Aruoja1, V.; Kahru, A.; Dubourguier, H. C. *Toxicol. Lett.* **2008**, *180S*, S220.
(13) Zhou, J.; Xu, N. S.; Wang, Z. L. *Adv. Mater.* **2006**, *18*, 2432.
(14) Guo, D. D.; Wu, C. H.; Jiang, H.; Li, Q. N.; Wang, X. M.; Chen, B. A. *J. Photochem. Photobiol., B* **2008**, *93*, 119.
(15) Vayssieres, L.; Keis, K.; Hagfeldt, A.; Lindquist, S. T. *Chem. Mater.* **2001**, *13*, 4395.
(16) Yang, H. G.; Zeng, H. C. *J. Phys. Chem. B* **2004**, *108*, 3492.
(17) Zhang, D. H.; Liu, Z. Q.; Han, S.; Li, C.; Lei, B.; Stewart, M. P.; Tour, J. M.; Zhou, C. W. *Nano Lett.* **2004**, *4*, 2151.

(18) Greene, L. E.; Law, M.; Tan, D. H.; Montano, M.; Goldberger, J.; Somorjai, G.; Yang, P. D. *Nano Lett.* **2005**, *5*, 1231.
(19) Liu, Z. W.; Ong, C. K.; Yu, T.; Shen, Z. X. *Appl. Phys. Lett.* **2006**, *88*, 053110.
(20) Bhatti, H. S.; Sharma, R.; Verma, N. K. *Radiat. Eff. Defects Solids* **2006**, *161*, 113.
(21) Guo, Y.; Cao, X. B.; Lan, X. M.; Zhao, C.; Xue, X. D.; Song, Y. Y. *J. Phys. Chem. C* **2008**, *112*, 8832.
(22) Oh, E.; Jung, S. H.; Lee, K. H.; Jeong, S. H.; Yu, S. G.; Rhee, S. J. *Mater. Lett.* **2008**, *62*, 3456.

JP903130T